A framework for testing computational models of endothelial cell network formation with *in vitro* time-lapses and a high-throughput image analysis pipeline

Tessa M. Vergroesen[1] and Roeland M.H. Merks[1,2]

[1]Institute of Biology Leiden, Leiden University, Leiden, The Netherlands
[2]Mathematical Institute, Leiden University, Leiden, The Netherlands

Abstract

The tube formation assay is a widely used *in vitro* method to evaluate the network-forming capacity of endothelial cells in a controlled environment. In this assay, endothelial cells rapidly self-organize into complex multicellular networks, enabling the study of processes such as cell-cell adhesion, connectivity, and motility. In parallel with experimental approaches, cell-based computational modelling can be used to help unravel what aspects of endothelial cell behavior suffice to explain the observed patterns of network formation. We have previously shown that time-lapse imaging in combination with systematic variation of culture conditions and simulation parameters is a useful tool in deciding between alternative model assumptions. Here, we present a detailed protocol for such systematic testing and falsifying computational models of endothelial cell network formation. This approach combines time-lapse imaging of *in vitro* network formation with simulated data from computational models, both analyzed using a quantitative image analysis pipeline. We describe methods for generating representative simulation data from published models, performing high-throughput *in vitro* experiments, and extracting morphological features through step-by-step image analysis. We also provide examples of downstream data analysis and feature-based comparisons between simulations and experimental time-lapse data. This protocol provides a framework to rigorously evaluate the predictive power and biological relevance of computational models of multicellular network formation.

Key words tube formation assay, image analysis, angiogenesis, model falsification, cellular Pott's model

Introduction

Vascular morphogenesis, including angiogenesis and vasculogenesis, is a fundamental process underlying tissue growth, repair, and homeostasis. It is tightly regulated and can be disrupted in diseases such as cancer, ischemia, and chronic inflammation [1–3]. During angiogenesis, endothelial cells (ECs) sprout from pre-existing vessels, migrate, proliferate, and organize into new vasculature [4]. While sprouting, ECs continuously sense and interact with their environment: chemically, by detecting signaling molecules such as VEGF-A [5, 6], and mechanically, by responding to the stiffness and composition of the extracellular matrix (ECM) [7–10]. Based on their position

within the sprout, ECs dynamically adapt their behavior and actively remodel their microenvironment. This adaptive behavior is central to vascular patterning and ensures efficient tissue perfusion [11].

The collective behavior of ECs during angiogenesis and vasculogenesis has been widely studied using *in vitro* network formation assays such as the 2D tube formation assay [12, 13]. In this assay, ECs are placed on an ECM-like substrate and spontaneously organize into multicellular networks [14, 15]. These networks are typically analyzed at a fixed point to assess the effects of experimental conditions on sprouting or network stability. However, endpoint measurements provide limited insight into the dynamic processes underlying network formation. Time-lapse imaging overcomes this limitation by enabling quantification of network development and feature evolution over time. This allows investigation of how cellular behaviors contribute to multicellular pattern formation and how perturbations such as genetic knockdowns or changes in the chemical or mechanical microenvironment affect angiogenic capacity.

In addition to experimental approaches, computational models are used to generate hypotheses and test whether (combinations of) biological mechanisms are sufficient to explain observed behaviors. Cell-based models, such as the cellular Potts model, simulate individual cell behavior and interactions, allowing assessment of whether current understanding of endothelial single cell dynamics is sufficient to reproduce the multicellular network structures and their temporal evolution observed *in vitro* [16]. However, a wide range of computational models incorporating different chemical and mechanical mechanisms can generate similar network morphologies. These include models based on chemoattraction [17–19], mechanical interactions [32, 35], cell-ECM communication [7, 20], contact-inhibition [18, 20], active cell elongation [17, 21], and the interaction with an elastic [22] or a fibrous [12, 34] ECM. Because multiple mechanistic hypotheses can produce comparable outcomes, it is essential to validate or falsify these models using experimental data.

In our previous work [23], we combined time-lapse imaging of the endothelial tube formation assay with a high-throughput image analysis pipeline to segment and quantify network features. By comparing dynamic features, such as branch length, connectivity, and network density, between experimental data and simulations, it becomes possible to assess which models capture the underlying processes of network formation and remodeling. Here, we present a detailed protocol for this integrated approach, combining 2D tube formation assays using immortalized human microvascular endothelial cells (HMEC-1), time-lapse widefield imaging, feature extraction in ImageJ, quantitative network analysis, and computational modelling. This workflow enables the extraction of structural features over time and facilitates the systematic comparison between experimental and simulated networks. The protocol provides a framework to test and falsify computational models of vascular morphogenesis and to evaluate their ability to reproduce the dynamic processes underlying endothelial network formation.

Materials

All solutions are prepared in a sterile environment, and consumable equipment should be sterilized prior to use.

Cell culture and tube formation assay

- Cell culture facility (Biosafety level 1) equipped with a laminar flow cabinet, a centrifuge for tubes and an incubator set to 5 % CO_2 and 37 °C.
- Complete EC medium: MCDB-131 medium without glutamine (*see* **Note 1**), supplemented with 10 mM L-alanyl-L-glutamine, 100 U/mL penicillin, 100 µg/mL streptomycin, 10% heat-inactivated fetal bovine serum (FBS); stored in 50 mL aliquots at 4 °C (*see* **Note 2**).
- Hydrocortisone (HC), 1 mg/ml in DMSO, stored in 100 µL aliquots at -20 °C.
- Human epidermal growth factor (hEGF), 10 µg/ml, stored in 100 µL aliquots at -20 °C.

- Immortalized human microvascular endothelial cells (HMEC-1) (*see* **Note 3**).
- Ibidi µ-Slide Angiogenesis used for 2D tube formation assays (*see* **Note 4**).
- Matrigel phenol red-free (*see* **Note 5**).
- Dulbecco's phosphate buffered saline (dPBS).
- Trypsin-EDTA working solution: 0.25 % (w/v) trypsin and 0.05 % (w/v) ethylenediaminetetraacetic acid (EDTA) in dPBS, stored in 2 mL aliquots at -20 °C (*see* **Note 6**).
- Optional for fluorescent labelling of the cells during life imaging: a cell staining of choice (*see* **Note 7**).
- Wide field microscope equipped with a motorized stage, a digital camera and a temperature, humidity and CO_2 controlled sample chamber (*see* **Note 8**).
- Microscope software which supports automatic image acquisition of multiple regions of interest over time, preferably with auto-focus or drift correction (*see* **Note 9**).

Image analysis

- A recent version of the ImageJ package Fiji [24] or an image analysis software of choice (*see* **Note 10**).
- Image analysis pipeline from https://github.com/TMVergroesen/NetworkAnalysis, which includes scripts to extract network information from *in vitro* time-lapses and computer simulations.
- A recent version of R [25] or a data visualization and analysis software of choice (*e.g.* GraphPad Prism or Python).

Computational modelling

- A computational model of multicellular network formation (*e.g.*, cellular Potts model) or a library of pre-generated simulation images (*see* **Note 11**).

Methods

Tube Formation Assay

All procedures should be completed under sterile conditions.

1. Grow cells to a confluency of approximately 80 % (*see* **Note 12**).
2. Thaw the Matrigel overnight on ice at 4 °C and place pipette tips in the fridge (*see* **Note 13**).
3. During the experiment, keep pipette tips, Matrigel and multi-well slide or plate on ice to prevent uneven polymerization of the Matrigel during preparation.
4. Gently homogenize the Matrigel by pipetting up and down without introducing air bubbles to the solution (*see* **Note 14**).
5. Add 10 µL Matrigel to the inner wells of the µ-slide through reverse pipetting (*see* **Note 15 and 16**).
6. Check the accuracy of the Matrigel volume by holding up the µ-slide and examining the breaking of light through the gel (*see* **Figure 1A**) (*see* **Note 17**).
7. Place slide at 37 °C for 30-60 min to gel the substrate (*see* **Note 18**).
8. Pre-warm EC medium and dPBS, and thaw Trypsin-EDTA (2 mL per 75 cm² flask).
9. Remove spent medium from culture flask.
10. Wash cells with dPBS (*see* **Note 19**).
11. Add 2 mL trypsin-EDTA per 75 cm² to completely cover the cells.
12. Place the flask at 37 °C for 5 min.
13. Check under the microscope if the cells have detached from the plate (*see* **Note 20**).
14. Add 4 mL complete medium per 75 cm² to stop the trypsin-EDTA reaction.
15. Collect all the liquid in a 15 mL conical tube.
16. Centrifuge the cell suspension for 5 min at 200-250 g at RT (*see* **Note 21**).

17. Carefully remove the supernatant by aspiration, without disturbing the pellet.
18. Resuspend the pellet in 1 mL fresh medium by gently pipetting up and down, minimizing shear stress.
19. Determine cell concentration with a hemocytometer or automated cell counter by mixing 10 µL cell suspension thoroughly with 10 µL Trypan blue (*see* **Note 22**).
20. Dilute to a final concentration of 2 x 10^5 cells per mL (*see* **Note 23**).
21. Add 50 µL cell suspension to each µ-slide well (*see* **Note 24**).
22. Add 27 µL medium to each well through reverse pipetting, ensure a dome of medium forms on top of the well (*see* **Figure 1B**) (*see* **Note 25 and 26**).
23. Gently place the lid on the slide.
24. Proceed to time-lapse acquisition.

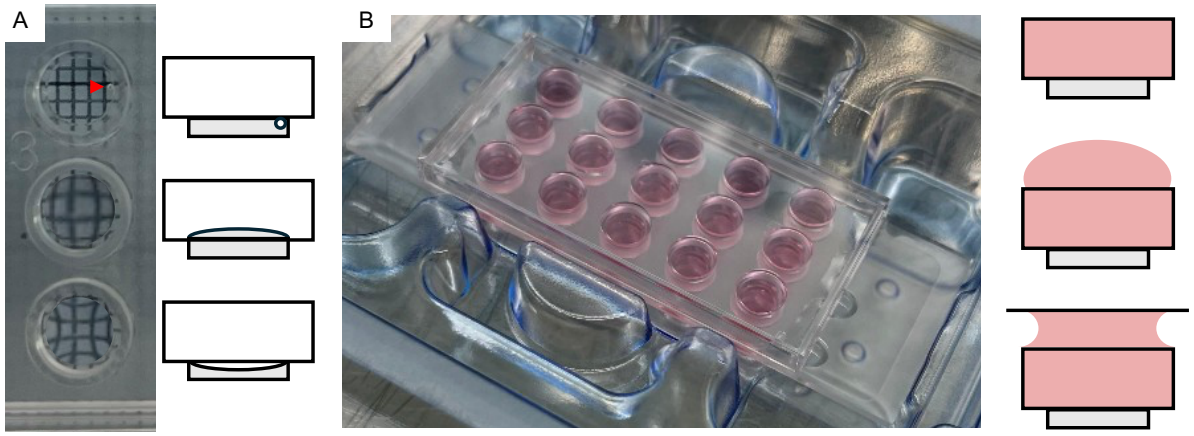

Figure 1. Preparing the ibidi slide. A) Examine if the Matrigel layer is flat and free of bubbles (red arrow) by placing the slide on top of a fine grid and checking for any warping of the lines. B) After seeding the cells, gently place a drop of medium on top of each full well to create a dome and ensure contact between the medium and the lid.

Time-lapse acquisition

Time-lapse images can be acquired using a live-cell imaging-compatible light microscope at preferred contrast settings and/or fluorescence suitable for life cell imaging (*e.g.* equipped with a humidified chamber, 37 °C incubation and 5 % CO_2). Here, we perform phase contrast imaging on a Zeiss Axio Observer 7, equipped with an Axiocam 705 mono camera and a 10× objective, and an ibidi stage top incubator.

1. Switch on the microscope and prewarm the sample stage to 37 °C at least 1 hour before imaging for temperature stabilization. Adjust the microscope incubator to 80 % humidity and 5% CO_2.
2. Place the sample slide in the holder (*see* **Note 27**).
3. Switch to a low magnification objective (*e.g.* 5×).
4. Select each slide well as a separate tile region and focus on the cells that have started to attach to the substrate (*see* **Note 28**).
5. Switch to the 10× objective and select the appropriate phase-contrast filter.
6. Adjust lamp brightness to 15-30 % and exposure time to 10-100 ms such that you have a clear contrast (*see* **Note 29**).
7. Adjust focus strategy to separately focus on the center of each well every timestep.
8. Enable automatic stitching after acquisition (*see* **Note 30**).
9. Setup time-lapse imaging for 24 hours with 15-minute intervals.
10. Run acquisition.

11. Save or export the time-lapse data to TIFF files containing full well time-lapse stacks for further processing (*see* **Note 31**).

Quantitative Analysis of Endothelial Network Formation

The following procedure describes how to quantify network morphology in *in vitro* tube formation assays using a Fiji macro (available at https://github.com/TMVergroesen/NetworkAnalysis). The macro performs segmentation, skeletonization, and branch and lacunae quantification, and generates annotated overview outputs in a semi-automated, high-throughput manner.

1. Start Fiji, install the macro script InVitro.ijm (*Plugins* → *Install…*) and restart Fiji.
2. When running the macro, found at the bottom of the Plugins menu, answer the prompts to adjust analysis preferences and set the image dimensions. These include image pixel size in micrometers (*e.g.* 1 µm), time interval between frames in minutes (*e.g.* 15 minutes), well diameter in micrometers (*e.g.* <4000 µm), well shape (circular or rectangular), and selection of (detailed) skeleton analysis, lacuna analysis, or both.
3. When prompted, select a directory containing image stacks (one time-lapse stack per well), and a directory for the output images and files.
4. If a directory with multi-channel images is provided, the macro automatically selects the brightest channel for automated image segmentation. If images exceed a predefined size threshold, they are resized to reduce memory usage. If a circular well is specified, the macro crops the central region, with the provided image dimensions as diameter (*see* **Figure 2A**) (*see* **Note 32**).
5. The endothelial network is segmented from the background using image sharpening, local intensity variance detection, and global thresholding followed by morphological filtering (*see* **Figure 2B**). Optional watershed segmentation can be enabled to connect weakly separated branches. The aim is to obtain an accurate binary representation of the cellular network (*see* **Figure 2B**).
6. If skeleton analysis is enabled, the binary image is skeletonized (*see* **Figure 2C**). The macro uses the *Analyze Skeleton* plugin to quantify the number, connectivity, and length of branches and junctions per frame. Additionally, detailed branch information can be enabled to separate the branches into sprouts (connected to a single node) and segments (connected to two nodes) using node connectivity.
7. If lacuna analysis is enabled, enclosed regions (lacunae) are detected, and their number, shape, and orientation are measured. The fraction of the area occupied by lacunae (i.e. the inverse of cell-covered area) is also calculated.
8. Results are saved automatically to the selected output directory. Outputs per time-lapse include:
    - Two CSV files, containing measurements of each lacuna and branch (*see* **Table 1 and 2**)
    - A CSV file summarizing both lacuna and branch features per frame (*see* **Table 3**)
    - An ROI set ZIP file containing outlines of the detected lacunae
    9. An annotated overview TIFF file showing the original time-lapse with overlays of the skeleton, lacunae outlines, junctions, and sprout endpoints (*see* **Figure 2E**)
10. Annotated overview images should be inspected to verify correct segmentation and identification of network structures (*see* **Figure 2E**) (*see* **Note 33**).

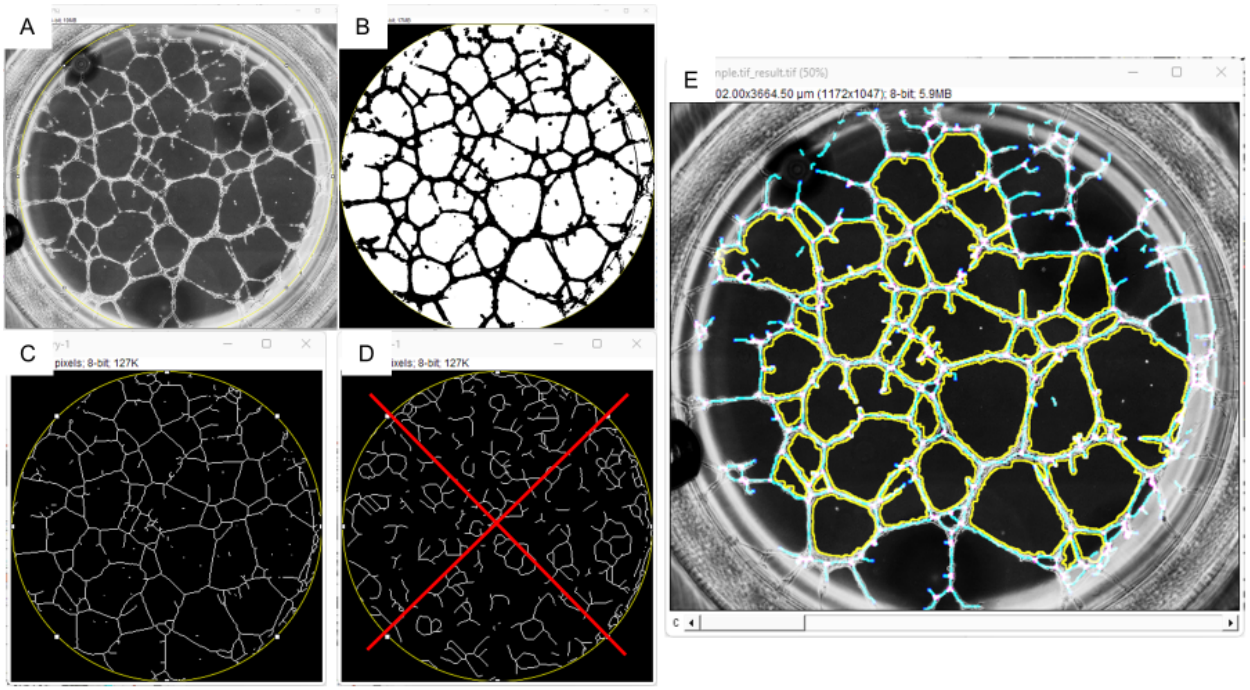

Figure 2. Image analysis pipeline. A) Phase-contrast image of a tube formation assay after 24 hours, displaying an endothelial cell network (white) on a Matrigel background (dark-grey). The selected circular well has a 4000 µm diameter. B) Binary image of the automatically segmented cell network. C) Binary image of the skeletonized cell network. D) Example of a segmentation error where the background is skeletonized instead of the network. E) Annotated overview image displaying the original phase contrast image overlaid with the lacuna outlines (yellow), network skeleton (cyan), nodes (magenta) and sprout endpoints (blue).

Table 1. Definition of lacuna features output file. In the individual lacuna features table, each row corresponds to an individual lacuna. The first rows correspond to lacunae in the earlier time frames and the last rows correspond to those of the later time frames. The columns contain the measures listed in this table.

Column header	**Explanation**
Label	Label of the image.
Area	Area of the specific lacuna (in µm²).
X, Y	Position of the lacuna centroid (in µm).
Perim.	Perimeter of the lacuna (in µm).
BX, BY	Position of the top left corner of the bounding box (an imaginary rectangular border drawn around the lacuna) (in µm).
Width, Height	The width and height of the lacuna bounding box (in µm).
Major, Minor	The longest and shortest diameters (in µm) of a best-fitting ellipse calculated over the lacuna. The major axis indicates the maximum length of the lacuna, while the minor axis represents the width perpendicular to it.
Angle	The orientation (0º to 180º) of the major axis relative to the x-axis of the image.
Circ.	The circularity of the lacuna, calculated as the lacuna area multiplied by 4π divided by the squared perimeter. A low circularity indicates a rough lacuna boundary.
%Area	The percentage of thresholded pixels within the selection (100% indicates the entire selected lacuna area is measured).
Slice	The frame number of the lacuna within the image stack.

AR	The aspect ratio of the lacuna, calculated as the length of the major axis of the lacuna divided by the minor axis length.
Round	The roundness of the lacuna, calculated as the area multiplied by 4, dividing by π times the squared major axis. A low roundness indicates a highly elongated shape.
Solidity	The solidity of the lacuna, calculated as the area divided by the area of its convex hull (an imaginary convex shape enclosing the lacuna).

Table 2. Definition of branch features output file. In the individual branch features table, each row corresponds to an individual branch. The first rows correspond to branches in the earlier time frames and the last rows correspond to those of the later time frames. The columns contain the measures listed in this table.

Column header	**Explanation**
Branch_time	The frame number of the specific branch.
Branch_x1	The x-coordinate of the start of the branch (in μm).
Branch_y1	The y-coordinate of the start of the branch (in μm).
Branch_x2	The x-coordinate of the end of the branch (in μm).
Branch_y2	The y-coordinate of the end of the branch (in μm).
Branch_length	The length of the branch (in μm).
Branch_type	The type of the branch. Branches are categorized as either segments, connecting two nodes, or spouts, connecting to only one node.

Table 3. Definition of summary features output file. In the summary features table, each row corresponds to a time frame of the time-lapse. The columns contain the cumulative and averaged measures listed in this table.

Column header	**Explanation**
Experiment	Title of the image.
Slice	The frame number of the row within the image stack.
Time	The frame number multiplied by the time interval (in hours).
Lacunae_n	The number of lacunae within the specified frame.
Lacunae_area	The average area of the lacunae within the frame (in μm²).
Lacunae_total_area	Position of the lacuna centroid (in μm).
Percentage	The percentage of the area of the ROI covered by lacunae, the inverse of the cell-covered area.
Major, Minor	The average longest and shortest diameters (in μm) of a best-fitting ellipse calculated over the lacunae.
Angle	The average orientation (0º to 180º) of the major axes of the lacunae. If this value differs substantially from 90º this may indicate that the overall network has some directionality.
Perimeter	The average perimeter of the lacunae (in μm).
Circularity	The average circularity of the lacunae.
Skeletons_n	The number of unconnected branch networks within the image frame.
Branches_length	The average length of the branches.
Branches_n	The number of branches within the frame.
Segments_length	The average length of the branches connected to two nodes.
Segments_n	The number of branches connected to two nodes.
Sprouts_length	The average length of the branches connected to only one node.
Sprouts_n	The number of branches connected to only one node.

Junctions_n	The number of nodes.
Triple_points_n	The number of nodes connected to three or four branches.
Branches_max_length	The length of the largest branch within the frame.
AreaB	The area of the ROI during the lacuna feature extraction.
AreaL	The area of the ROI during the branch feature extraction.

Computational Modelling of Network Formation

1. Select a suitable computational model for vascular network formation (*e.g.*, a cellular Potts, or a continuum model) according to the research question. As an example, a cellular Potts model (CPM) can be used to simulate endothelial cell behavior during network formation (*e.g.* [17, 18, 22]).
2. Initialize model parameters to approximate experimental conditions, including initial cell number (matching the number of cells per *in vitro* well), cell target area and length (based on measured cell dimensions), adhesion energies (reflecting cell-cell and cell-ECM interactions), and simulation domain size (corresponding to the physical well size).
3. Configure model output to generate 2D images that can be processed like the *in vitro* stacks. Alternatively, export quantitative network descriptors directly from the simulation code (*e.g.*, branch length, lacuna area, and junction counts) that are comparable to those obtained from the image analysis pipeline.
4. Run simulations according to the model documentation (*see* **Note 34**).
5. Start Fiji and open the macro script InSilico.ijm (*File* → *Open…*).
6. Before running the macro, adjust analysis parameters in the header of the script if needed. These include simulation time steps (*e.g.* number of Monte Carlo steps between images), image extension (*e.g.* .tif or .png), pixel size, well diameter, well shape, selection of skeleton analysis, lacuna analysis, or both.
7. Similarly to the *in vitro* feature extraction, the results are saved automatically to the selected output directory.

Comparison between model and experiment

This section describes a workflow for comparing *in vitro* and *in silico* data using R.

1. Import summarizing CSV files into R (*e.g.*, using the functions fread or read.csv) (*see* **Note 35**).
2. Visualize time-resolved features using ggplot2 to assess qualitative agreement between *in vitro* and *in silico* data. Evaluate whether the model reproduces the characteristic phases and temporal dynamics of network formation (*see* **Figure 3**) (*see* **Note 36**).
3. Perform a structured comparison between model and experiments. For example, *in vitro* networks typically undergo aggregation, network formation, and remodeling within 24 hours under standard assay conditions. Simulations should therefore be run for sufficient time to determine whether similar phases emerge and to identify the simulation step at which transitions between these phases occur. Compare both the timing of phase transitions and the corresponding network characteristics, including branch density and length, lacuna number and size, and their variability and spatial distribution (*see* **Figure 3A**).
4. Adjust the model parameters where biologically justifiable, based on observed discrepancies. Examples include:
    - increase or decrease the cell-cell adhesion strength to modulate cell aggregation
    - alter the chemotactic sensitivity to influence sprouting behavior and network connectivity
    - modify the cell area or length constraints to affect cell morphology and heterogeneity
    - adjust ECM interaction parameters to influence network stability

    Parameter changes should be recorded as part of a systematic sensitivity or parameter sweep rather than *ad hoc* tuning (*see* **Note 37**). For example, increasing the chemokine diffusion length in the model shown

in **Figure 3B** improved agreement with experimental network characteristics (*see* **Figure 3C-G**), illustrating how systematic parameter exploration can be used to identify biologically plausible parameter regimes.

5. Model evaluation is based on the ability of a model to reproduce experimentally observed network formation dynamics within biologically realistic parameter ranges (*see* **Figure 3**). A model may require revision or rejection if it consistently fails to reproduce:
    - the correct ordering and timing of network formation phases
    - characteristic temporal trends in network features, including branch density, lacuna density, and lacuna area
    - the magnitude, variability, and spatial organization of network features
    - responses to parameter perturbations

    Model performance should be assessed using quantitative error metrics (e.g., mean squared deviation of feature curves or correlation-based measures), rather than visual inspection alone.

Final remarks on model falsification

If a model fails to adequately reproduce the experimental data for any parameter regime, model assumptions should be revisited, including the choice of interaction rules, signaling mechanisms, or mechanical representations of the ECM. This may involve introducing additional biological mechanisms (e.g., contact inhibition, matrix remodeling, or heterogeneity in cell population). Conversely, models that successfully reproduce the observed dynamics should be evaluated under additional conditions, such as alternative cell densities, ECM compositions, mechanism knockouts or other perturbations. Agreement under a single condition is insufficient to validate a model; some robustness is required to support mechanistic validity. Although this protocol is described using HMEC-1-based tube formation assays compared to a cellular Potts model, the same workflow can be adapted to other endothelial or non-endothelial cell cultures by modifying cell-specific parameters (e.g., adhesion, motility) in the model and including additional feature extraction pipelines. The general framework remains applicable to any system in which emergent multicellular structures can be quantified over time. Overall, this approach implements an iterative systems biology cycle of hypothesis generation, simulation, experimental validation, and model refinement to progressively identify missing or incorrect mechanistic assumptions.

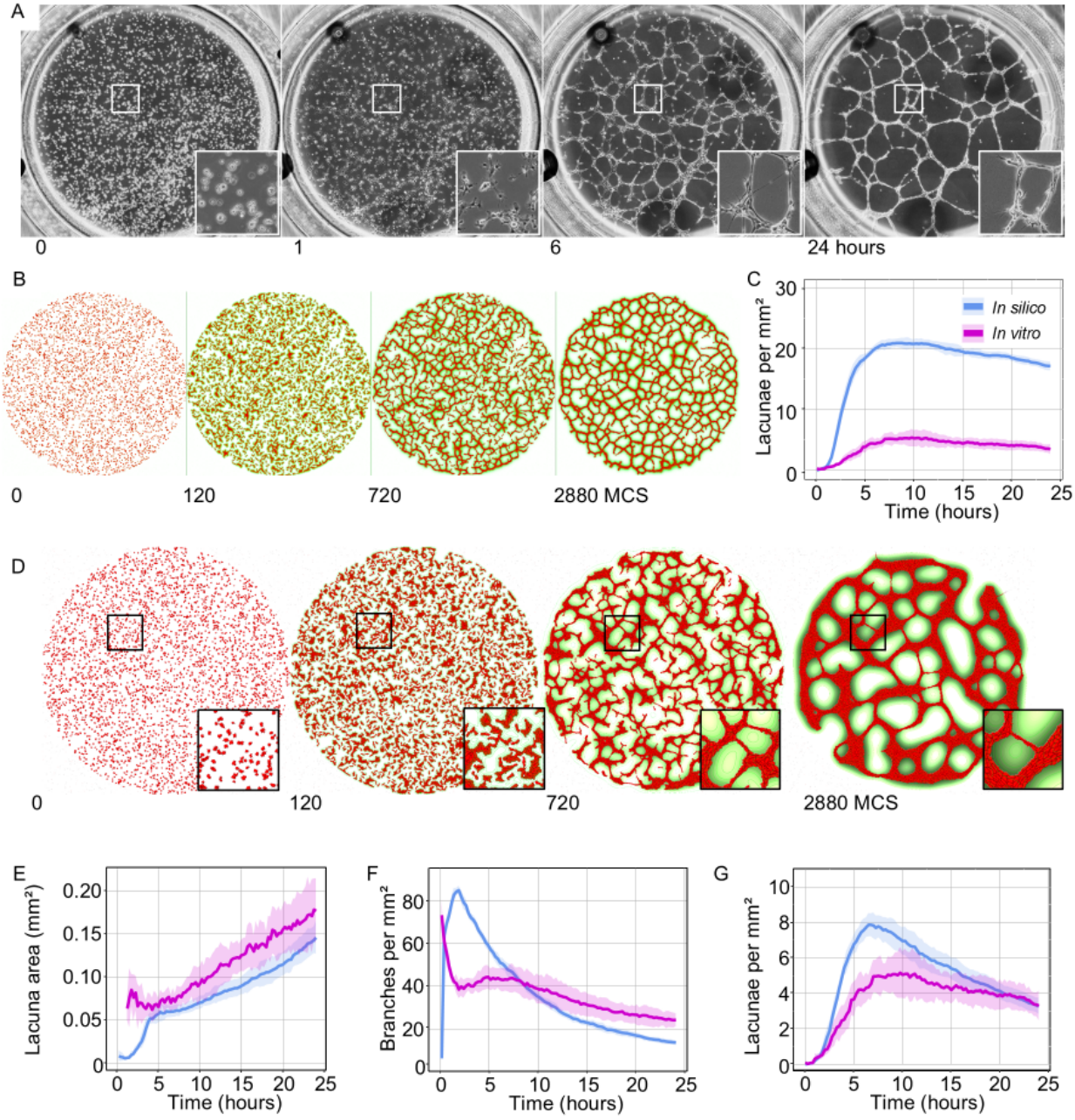

Figure 3. *In vitro-in silico* comparison. A) Phase-contrast images of an *in vitro* tube formation assay at 0, 1, 6 and 24 hours. B) Representative simulation output of a cellular Potts model of endothelial network formation at 0, 120, 720 and 2880 Monte Carlo steps (MCS). Cells (red) secrete a chemoattractant (green) which diffuses through the medium (white). C) Lacuna density for simulation outputs similar to the example shown in B (blue), compared to experimental observations (magenta). D) Representative simulation output with a longer diffusion length relative to the example shown in B. E-G) Quantitative comparison of E) lacuna area, F) branch density, and G) lacuna density over time for simulation outputs similar to the example shown in D (blue) compared to experimental data (magenta). A, C, E-G adjusted from [23].

Notes

1. For culturing immortalized human microvascular endothelial cells (HMEC-1), we use MCDB-131 medium. For the best results, use the recommended medium and necessary supplements for the endothelial cell line of choice (*e.g.* EGM-2 for HUVECs).

2. Since FBS has a limited shelf life after thawing (2-4 weeks), it is recommended to make smaller complete EC medium aliquots to be stored at 4 °C, which can be consumed within this time.
3. Choose the appropriate endothelial cell line for your experiment. HMEC-1 cells are robust, proliferate consistently, and form reproducible networks, making them suitable for tube formation assays. Adjust culture conditions accordingly for other cell lines.
4. In this protocol we will focus on how to analyze the time-lapse images of the EC network formation in a high throughput manner. We used the ibidi µ-Slide Angiogenesis as we deemed it most suitable for high-throughput whole well imaging, but we will suggest protocol adjustments for different multi-well plates, single wells or slides.
5. Phenol red in Matrigel can contribute background fluorescence. Other substrates than Matrigel can also be used (*e.g.* Geltrex or synthetic alternatives [26, 27]).
6. EDTA is not essential for cell detachment during passaging. However, the EDTA will increase the trypsin efficacy and reduce cell clumping. Cells can also be detached using a cell scraper, if preferred.
7. It is important to select a live-cell stain that does not significantly affect endothelial network formation. For example, CellTracker dyes have been shown to work effectively in short term experiments [28], and membrane linkers such as PKH or CellVue do not alter network formation when used at low concentrations [29].
8. Here, we use a Zeiss Axio Observer 7 microscope equipped with an Axiocam 705 mono camera, EC Plan-Neofluar objectives (5× and 10×), and a Colibri 7 solid-state light source with LED excitation (385–630 nm) and appropriate filter sets. However, the protocol is compatible with other wide-field microscopes that provide stable live-cell imaging with environmental control, motorized stage, and automated acquisition.
9. If the microscope software does not include features such as multi-region acquisition, auto-focus, or tile stitching, the protocol can still be followed. However, this will limit throughput and/or increase manual labor. Matrigel contraction or expansion over time may cause the substrate surface to drift out of focus during long time-lapse experiments. Taking a Z-stack compensates for this drift, but this will increase image acquisition time and reduce the potential for high-throughput experiments.
10. For image analysis, we provide a Fiji/ImageJ macro script that automates segmentation, skeletonization, and quantification of endothelial networks in 2D time-lapse images. For this we used ImageJ version 1.54. Alternatively, other software packages such as Python (with scikit-image [30] and OpenCV [31]) or MATLAB (with the Image Processing Toolbox [32]) can be used to perform similar analyses.
11. Several computational approaches can simulate network formation. Cellular Potts models (*e.g.*, Tissue Simulation Toolkit [33], CompuCell3D [34], Morpheus [35]) and agent-based models capture individual cell behaviors and interactions, while continuum or hybrid models describe cell densities and cytokine concentrations in space. Libraries like the Tissue Simulation Toolkit (TST) provide C++ functions for custom simulations, whereas platforms such as Morpheus and CompuCell3D allow model setup and execution via graphical interfaces. Tool choice depends on model complexity and desired customization. Model inputs should reflect experimental conditions and the hypotheses for endothelial network formation that are being tested, and outputs should generate network descriptors comparable to image analysis for direct quantitative comparison.
12. Cells should reach approximately 80% confluency. Overconfluent cultures begin to differentiate, altering proliferation and network formation [36]. Some staining protocols may require a slightly different confluency; however, maintain consistency across experiments, as confluency influences the resulting network morphology.
13. Thaw Matrigel slowly on ice at 4 °C, preferably overnight. Rapid thawing or warming can cause premature gelation, compromising uniform coating and reproducibility.

14. If bubbles form, briefly centrifuge the Matrigel at low speed to remove them, as air pockets in the substrate can disrupt tube formation. Then, gently pipette up and down using cooled pipette tips to homogenize the solution before proceeding.
15. Fully expelling the pipette could introduce air bubbles in the Matrigel substrate. For as long as the slide remains on ice, the Matrigel should not polymerize. If bubbles appear, aspirate the Matrigel from the well and refill it more carefully. Use reverse pipetting where you over-aspirate and expel only to the first stop without fully expelling to improve accuracy and prevent bubble formation. Support your pipetting hand with your other hand or a pipette tip box to avoid touching the wall of the well while expelling the Matrigel.
16. For microscopy slides or regular multi-well plates there are multiple options available to prevent a substrate meniscus from forming and to achieve a flat Matrigel layer. Namely, for small wells, one could simply increase the Matrigel volume (100 µL per cm^2) and restrict the image area to the center of the wells. For larger wells, less volume (50 µL per cm^2) will result in a flatter layer. The slide or plate can also be centrifuged briefly to achieve a more uniform layer. Another option would be to try placing a hydrophobic coverslip on top of the substrate, which can be carefully removed after gel polymerization.
17. Place the µ-slide on a fine grid and examine how light passes through the substrate. If the grid appears distorted, the added volume may be too high or too low. An undistorted grid indicates the correct volume. If a meniscus has formed in the well, carefully remove the unpolymerized substrate and refill the well with the adjusted volume.
18. Ensure that the Matrigel polymerizes completely, or increase incubation time. Avoid moving the slide during this period, as vibrations or tilting can create uneven surfaces or bubbles that disrupt subsequent tube formation. Avoid incubating the polymerized substrate too long, as the substrate can dry out. Medium or sterile dPBS can be added to the substrate after polymerization to prevent drying out.
19. Cell staining should be performed directly on the adherent monolayer, before detachment. Staining cells while they remain attached is generally less disruptive than staining cells in suspension, helping to preserve cellular morphology and reducing stress-induced changes that could affect subsequent network formation. Follow procedure for the staining of choice.
20. If cells are partially detached after incubation with trypsin-EDTA, gently tap or rock the flask to encourage detachment. Avoid leaving the cells in trypsin for more than 10 minutes, as prolonged exposure can damage cell membranes and affect subsequent tube formation assays.
21. Centrifuge gently to form a compact cell pellet without causing mechanical stress. Excessive g-force or prolonged centrifugation can damage endothelial cells and reduce viability. If the pellet is loose, lower the brake speed of the centrifuge.
22. When determining cell concentration, ensure thorough mixing with Trypan blue to accurately distinguish viable from non-viable cells (pipette up and down >30 times). Inconsistent mixing can lead to under- or overestimation of cell density, which may impact network formation in downstream assays. Avoid creating bubbles, as these can interfere with accurate counting.
23. The final cell concentration in this example is chosen to seed 10,000 cells per well with a 50 µL suspension. This corresponds to a concentration of 2×10^5 cells per mL. The concentration can be adjusted depending on desired cell density or well volume. Always mix the suspension gently to ensure homogeneity before pipetting.
24. To ensure even cell distribution, gently dispense the medium as a droplet from the pipette tip onto the center of the well. Avoid dispersing the suspension with excessive force, as this can create uneven seeding. If testing cytokines or other experimental factors, pre-mix them into the medium prior to addition to the well. Introducing experimental factors at this stage ensures homogeneous exposure during early network formation, which is critical for reproducible tube formation.

25. Be careful not to touch the medium domes or shake the slide, to avoid the medium from spilling over the well. If a spill does occur, aspirate the medium from the slide fully before recreating the dome. If cells are unevenly distributed at the start of the experiment, incubate the slide for 30 minutes before adding the medium domes. This allows the cells to attach to the substrate and helps prevent cell displacement during the addition of the medium domes.
26. Although 25 µL of medium is sufficient to form a dome that makes contact with the lid, using 27 µL provides extra volume so that mild evaporation during the time-lapse does not immediately break the medium column from the lid to the sample. Maintaining contact between the medium and the lid ensures uninterrupted homogeneous light passage from lid to sample for optimal phase contrast imaging. Minor evaporation can still occur during long time-lapses, so use a humidified chamber and place drops of sterile PBS or water in the corners of the slide. If evaporation still occurs, add water basins to the microscope chamber to further reduce evaporation.
27. A temperature mismatch between the sample and the humidified microscope chamber can lead to condensation on the sample slide. To minimize condenstation, pre-warm the slide to 37 °C before inserting it into the microscope chamber.
28. Align the well precisely at the center of the imaging tile to ensure accurate automatic analysis of the network. Focus on already attached cells - in phase contrast these look like a fried egg – Since all endothelial cells will eventually spread during attachment this will ensure optimal focus throughout the time-lapse. Alternatively, acquiring a small z-stack at each time point can correct for variations in substrate height, but doing so will increase acquisition time and file size.
29. Adjust lamp brightness and exposure time to achieve clear contrast without saturating the bit-depth of the image. Excessive illumination can cause phototoxicity, while too dim light reduces segmentation accuracy during analysis. If possible, adjust imaging setup to keep the lamp on during acquisition of a single timestep to increase speed.
30. Check that automatic stitching aligns the tiles correctly. Misalignment can distort network measurements, so visually inspect time points before full analysis. Adjust tile-overlap or autofocus settings if needed. If automated stitching is not available, stitching can be performed using plugins in Fiji (*Plugins* → *Stitching*). Alternatively, single tiles may be analyzed; however, in this case, using a lower magnification objective is recommended to increase the field of view and minimize loss of network structures outside the imaging area.
31. Microscopy software usually provides users with an autosave option where it saves the data as one big file (*e.g.* .CZI, .ND2, .LIF, .OIR). These can be imported into ImageJ via the Bioformats importer. However, for downstream processing it is convenient to export the individual time-lapse stacks to separate TIFF files.
32. TIFF files containing multiple frames and channels can be large (>1 GB). Opening a TIFF as virtual stack reduces memory usage but slows processing. Therefore, the memory allocation in ImageJ can be adjusted via *Edit* → *Options* → *Memory & Threads…*, according to the available system working memory.
33. Correct identification of network features typically shows skeletons along visible cellular branches. If the background has been skeletonized instead, invert the image before skeletonization by adding the line 'run("Invert", "stack");' to the macro (*see* **Figure 2C and 2D**). This also applies when the lacuna ROIs outline the branches in the binary image instead of the lacunae. If there is too much noise present in the segmentation, pre-filter the time-lapses with either a median or a Gaussian filter. If the network is under segmented, remove or dial down any of the filter steps currently present in the macro.
34. When generating a lot of simulation data, it is essential to store all model parameters, including random seeds for each simulation. For reproducibility it is also important to keep track of model versions, either by storing a copy of the source code with the simulation output, or by labelling output by date and keeping track of versions via GitHub.

35. When importing the data it can be convenient to store multiple sets in one data table or data frame. This can be done by binding the different sets together using 'rbindlist'. The column containing the image name can then be used as a grouping factor in downstream data processing.
36. The 'ggplot2' function 'geom_smooth' can be used to quickly assess the overall trend of the dataset. However, smoothing may obscure short-term fluctuations or rapid changes in network features and should therefore be interpreted alongside the raw data.
37. Parameter adjustment should be guided by biological hypotheses rather than solely by improving agreement with experimental data. Improving agreement with experimental observations is only meaningful when parameter changes correspond to biologically justified mechanisms.

Acknowledgements

This work is part of the 'Mathematics-based strategies for repairing tumor blood vessels' project with project number 865.17.004 to RM of the Vici research program which is financed by the Dutch Research Council (https://www.nwo.nl/). The authors have no conflicts of interest to declare that are relevant to the content of this chapter.

References

1. Boey E, Zaidi H, Tang T, Yazdanyar A (2025) Role of Angiogenesis in Retinal Diseases and New Advances in Drug Development. Cells 14:1849. https://doi.org/10.3390/cells14231849
2. Folkman J (1995) Angiogenesis in cancer, vascular, rheumatoid and other disease. Nat Med 1:27–31. https://doi.org/10.1038/nm0195-27
3. Hanahan D (2022) Hallmarks of Cancer: New Dimensions. Cancer Discov 12:31–46. https://doi.org/10.1158/2159-8290.CD-21-1059
4. Risau W (1997) Mechanisms of angiogenesis. Nature 386:671–674. https://doi.org/10.1038/386671a0
5. Gerhardt H, Golding M, Fruttiger M, Ruhrberg C, Lundkvist A, Abramsson A, Jeltsch M, Mitchell C, Alitalo K, Shima D, Betsholtz C (2003) VEGF guides angiogenic sprouting utilizing endothelial tip cell filopodia. J Cell Biol 161:1163–1177. https://doi.org/10.1083/jcb.200302047
6. Lee C, Kim M-J, Kumar A, Lee H-W, Yang Y, Kim Y (2025) Vascular endothelial growth factor signaling in health and disease: from molecular mechanisms to therapeutic perspectives. Sig Transduct Target Ther 10:170. https://doi.org/10.1038/s41392-025-02249-0
7. Tranqui L, Tracqui P (2000) Mechanical signalling and angiogenesis. The integration of cell–extracellular matrix couplings. Comptes Rendus de l'Académie des Sciences - Series III - Sciences de la Vie 323:31–47. https://doi.org/10.1016/S0764-4469(00)00110-4
8. Manoussaki D, Lubkin SR, Vernon RB, Murray JD (1996) A mechanical model for the formation of vascular networks in vitro. Acta Biotheor 44:271–282. https://doi.org/10.1007/BF00046533
9. Manoussaki D (2003) A mechanochemical model of angiogenesis and vasculogenesis. ESAIM: M2AN 37:581–599. https://doi.org/10.1051/m2an:2003046
10. Califano JP, Reinhart-King CA (2009) The effects of substrate elasticity on endothelial cell network formation and traction force generation. In: 2009 Annual International Conference of the IEEE Engineering in Medicine and Biology Society. pp 3343–3345
11. Trimm E, Red-Horse K (2023) Vascular endothelial cell development and diversity. Nat Rev Cardiol 20:197–210. https://doi.org/10.1038/s41569-022-00770-1
12. DeCicco-Skinner KL, Henry GH, Cataisson C, Tabib T, Gwilliam JC, Watson NJ, Bullwinkle EM, Falkenburg L, O'Neill RC, Morin A, Wiest JS (2014) Endothelial Cell Tube Formation Assay for the In Vitro Study of Angiogenesis. J Vis Exp 51312. https://doi.org/10.3791/51312

13. Kelley M, Fierstein S, Purkey L, DeCicco-Skinner K (2022) Endothelial Cell Tube Formation Assay: An In Vitro Model for Angiogenesis. In: Fiedler LR, Pellet-Many C (eds) VEGF Signaling: Methods and Protocols. Springer US, New York, NY, pp 187–196
14. Nowak-Sliwinska P, Alitalo K, Allen E, Anisimov A, Aplin AC, Auerbach R, Augustin HG, Bates DO, van Beijnum JR, Bender RHF, Bergers G, Bikfalvi A, Bischoff J, Böck BC, Brooks PC, Bussolino F, Cakir B, Carmeliet P, Castranova D, Cimpean AM, Cleaver O, Coukos G, Davis GE, De Palma M, Dimberg A, Dings RPM, Djonov V, Dudley AC, Dufton NP, Fendt S-M, Ferrara N, Fruttiger M, Fukumura D, Ghesquière B, Gong Y, Griffin RJ, Harris AL, Hughes CCW, Hultgren NW, Iruela-Arispe ML, Irving M, Jain RK, Kalluri R, Kalucka J, Kerbel RS, Kitajewski J, Klaassen I, Kleinmann HK, Koolwijk P, Kuczynski E, Kwak BR, Marien K, Melero-Martin JM, Munn LL, Nicosia RF, Noel A, Nurro J, Olsson A-K, Petrova TV, Pietras K, Pili R, Pollard JW, Post MJ, Quax PHA, Rabinovich GA, Raica M, Randi AM, Ribatti D, Ruegg C, Schlingemann RO, Schulte-Merker S, Smith LEH, Song JW, Stacker SA, Stalin J, Stratman AN, Van de Velde M, van Hinsbergh VWM, Vermeulen PB, Waltenberger J, Weinstein BM, Xin H, Yetkin-Arik B, Yla-Herttuala S, Yoder MC, Griffioen AW (2018) Consensus guidelines for the use and interpretation of angiogenesis assays. Angiogenesis 21:425–532. https://doi.org/10.1007/s10456-018-9613-x
15. Arnaoutova I, Kleinman HK (2010) In vitro angiogenesis: endothelial cell tube formation on gelled basement membrane extract. Nat Protoc 5:628–635. https://doi.org/10.1038/nprot.2010.6
16. Merks RMH, Glazier JA (2005) A cell-centered approach to developmental biology. Physica A: Statistical Mechanics and its Applications 352:113–130. https://doi.org/10.1016/j.physa.2004.12.028
17. Merks RMH, Brodsky SV, Goligorksy MS, Newman SA, Glazier JA (2006) Cell elongation is key to in silico replication of in vitro vasculogenesis and subsequent remodeling. Dev Biol 289:44–54. https://doi.org/10.1016/j.ydbio.2005.10.003
18. Merks RMH, Perryn ED, Shirinifard A, Glazier JA (2008) Contact-Inhibited Chemotaxis in De Novo and Sprouting Blood-Vessel Growth. PLOS Computational Biology 4:e1000163. https://doi.org/10.1371/journal.pcbi.1000163
19. Serini G, Ambrosi D, Giraudo E, Gamba A, Preziosi L, Bussolino F (2003) Modeling the early stages of vascular network assembly. EMBO J 22:1771–1779. https://doi.org/10.1093/emboj/cdg176
20. Vega R, Carretero M, Travasso RDM, Bonilla LL (2020) Notch signaling and taxis mechanisms regulate early stage angiogenesis: A mathematical and computational model. PLOS Computational Biology 16:e1006919. https://doi.org/10.1371/journal.pcbi.1006919
21. Palm MM, Merks RMH (2013) Vascular networks due to dynamically arrested crystalline ordering of elongated cells. Phys Rev E 87:012725. https://doi.org/10.1103/PhysRevE.87.012725
22. van Oers RFM, Rens EG, LaValley DJ, Reinhart-King CA, Merks RMH (2014) Mechanical Cell-Matrix Feedback Explains Pairwise and Collective Endothelial Cell Behavior In Vitro. PLOS Computational Biology 10:1–14. https://doi.org/10.1371/journal.pcbi.1003774
23. Vergroesen TM, Vermeulen V, Merks RMH (2025) Falsifying computational models of endothelial cell network formation through quantitative comparison with in vitro models. PLOS Computational Biology 21:e1012965. https://doi.org/10.1371/journal.pcbi.1012965
24. Schindelin J, Arganda-Carreras I, Frise E, Kaynig V, Longair M, Pietzsch T, Preibisch S, Rueden C, Saalfeld S, Schmid B, Tinevez J-Y, White DJ, Hartenstein V, Eliceiri K, Tomancak P, Cardona A (2012) Fiji: an open-source platform for biological-image analysis. Nat Methods 9:676–682. https://doi.org/10.1038/nmeth.2019
25. RStudio Team (2022) RStudio: Integrated Development Environment for R
26. Aisenbrey EA, Murphy WL (2020) Synthetic alternatives to Matrigel. Nat Rev Mater 5:539–551. https://doi.org/10.1038/s41578-020-0199-8
27. Faulkner A, Purcell R, Hibbert A, Latham S, Thomson S, Hall WL, Wheeler-Jones C, Bishop-Bailey D (2014) A thin layer angiogenesis assay: a modified basement matrix assay for assessment of endothelial cell differentiation. BMC Cell Biol 15:41. https://doi.org/10.1186/s12860-014-0041-5
28. Kempers L, Bijl I van der, Stalborch A-MD van, Ponsioen B, Margadant C (2021) Fast in vitro protocol for the visualization and quantitative high-throughput analysis of sprouting angiogenesis by confocal microscopy. STAR Protocols 2:100690. https://doi.org/10.1016/j.xpro.2021.100690

29. Parsa H, Upadhyay R, Sia SK (2011) Uncovering the behaviors of individual cells within a multicellular microvascular community. Proc Natl Acad Sci U S A 108:5133–5138. https://doi.org/10.1073/pnas.1007508108

30. Walt S van der, Schönberger JL, Nunez-Iglesias J, Boulogne F, Warner JD, Yager N, Gouillart E, Yu T (2014) scikit-image: image processing in Python. PeerJ 2:e453. https://doi.org/10.7717/peerj.453

31. Bradski G (2000) The OpenCV Library. Dr Dobb's Journal of Software Tools

32. The MathWorks Inc (2025) Image Processing Toolbox. Natick, Massachusetts, United State

33. Daub JT, Merks RMH (2015) Cell-Based Computational Modeling of Vascular Morphogenesis Using Tissue Simulation Toolkit. In: Ribatti D (ed) Vascular Morphogenesis: Methods and Protocols. Springer, New York, NY, pp 67–127

34. Swat MH, Thomas GL, Belmonte JM, Shirinifard A, Hmeljak D, Glazier JA (2012) Multi-Scale Modeling of Tissues Using CompuCell3D. Methods in cell biology 110:325. https://doi.org/10.1016/B978-0-12-388403-9.00013-8

35. Starruß J, de Back W, Brusch L, Deutsch A (2014) Morpheus: a user-friendly modeling environment for multiscale and multicellular systems biology. Bioinformatics 30:1331–1332. https://doi.org/10.1093/bioinformatics/btt772

36. Yoshino D, Funamoto K, Sato K, Kenry, Sato M, Lim CT (2020) Hydrostatic pressure promotes endothelial tube formation through aquaporin 1 and Ras-ERK signaling. Commun Biol 3:152. https://doi.org/10.1038/s42003-020-0881-9